Temperature dependence of the magnetic excitations in gadolinium

J. W. Cable, R. M. Nicklow, and N. Wakabayashi*

Solid State Division, Oak Ridge National Laboratory, Oak Ridge, Tennessee 37831

The magnetic excitation spectra of Gd were measured out to the zone boundaries in the $\langle h00 \rangle$ and $\langle 00l \rangle$ directions over the temperature range from 9 to 320 K. The $\langle h00 \rangle$ data were not analyzed because of technical complications, but the $\langle 00l \rangle$ data are described remarkably well over the entire q and T range of the experiments by a damped-harmonic-oscillator form for the spectral weight function. The $\langle 00l \rangle$ data were parametrized and placed on an absolute basis by an internal calibration using the energy-integrated intensities of the low-temperature spin waves. This parametrization and calibration of the data provide a description of both the static and dynamic spin correlations over this temperature range. Spin-wave peaks are not observed above T_c in the $\langle 00l \rangle$ direction. We attribute this result to the low spin-excitation energies relative to $k_B T_c$ in this direction.

I. INTRODUCTION

There is considerable current interest in the spin fluctuations of ferromagnets at finite temperatures, particularly for $T > T_c$. Much of this interest centers around the itinerant magnets Fe and Ni, where controversy has developed regarding the presence of propagating spin-wave modes above T_c and the implications these may have regarding the degree of magnetic short-range order in the paramagnetic region.[1] Shirane et al.[2,3] contend that the spin fluctuations of Fe and Ni above T_c can be explained by spin-diffusion theory while Mook and Lynn[4,5] maintain that there is a crossover from diffusive to damped spin-wave behavior at energies $\hbar\omega$ greater than $k_B T_c$. Quite generally, the spin fluctuations at small wave vectors q reflect the macroscopic magnetic behavior while the large-q fluctuations depend on the nearest-neighbor interactions. The situation is fairly well understood for the Heisenberg paramagnet where most of the theoretical effort has been directed.[6-11] Here, there is a crossover from spin diffusion at small q to damped spin-wave behavior at large q. Similar behavior is calculated[12] for Fe by use of the Heisenberg model with the effective exchange constants taken from band calculations. However, the calculated peaks in constant-q scans occur at larger q and ω values than those reported by Mook and Lynn.[5] The spin fluctuations of a system define the magnetic behavior which has different characteristics for different classes of magnetic materials. For a better understanding of the different classes of magnetic materials, it is important to study the spin fluctuations over as broad a q, T, and ω range as possible for a wide variety of materials. It should be realized that these are very difficult measurements for the itinerant magnets, which have very steep dispersion curves, and measurements above T_c have been made for q values only about one-quarter of the way to the zone boundary. The neutron measurements are much easier for the Heisenberg ferromagnets which have relatively low spin-wave energies, and data have been obtained out to the zone boundaries for EuO,[13] EuS,[14] and

Gd.[15] Spin-wave-like excitations are reported in constant-q scans for temperatures up to $2T_c$ for EuO and EuS and to about $1.2T_c$ for Gd.

In this paper we describe measurements of the spin fluctuations in metallic Gd carried out by inelastic-neutron-scattering methods. In many ways, Gd is an ideal candidate for such studies. The Gd behaves as a tripositive, S-state ion so that anisotropy is small and the energetics are dominated by the exchange interactions. The $4f$ electrons are well localized so that the Heisenberg model should apply. Furthermore, it is a simple ferromagnet with a convenient Curie temperature of 292.7 K. However, isotopic samples must be used to avoid the high absorption cross section of natural Gd. More serious complications are the features that make theoretical comparisons with the data difficult. These include a uniaxial hcp crystal structure ($a_0 = 3.634$ Å and $c_0 = 5.781$ Å) and long-ranged exchange interactions. However, the effective interatomic exchange interactions have been extracted[16] from the low-temperature spin-wave dispersion data[17] so that Heisenberg-model calculations are feasible.

II. THEORY

The partial differential cross section for magnetic scattering from a Heisenberg ferromagnet is given by[18]

$$
\frac{d^2\sigma}{d\Omega\,dE} = \left[\frac{e^2\gamma}{mc^2} \right]^2 f^2(\mathbf{Q}) \frac{k'}{k} \omega(n_\omega + 1)
$$

$$
\times \sum_\alpha (1 - \hat{Q}_a^2) S^\alpha(\mathbf{Q}, \omega) , \tag{1}
$$

where the energy transfer is $\hbar\omega = E - E'$, $\mathbf{k}$ and $\mathbf{k}'$ are the incident and scattered neutron wave vectors, and the scattering vector $\mathbf{Q}$ is defined by $\mathbf{Q} = \mathbf{k} - \mathbf{k}'$. The Bose factor is given by $n_\omega = [\exp(\hbar\omega\beta) - 1]^{-1}$, where $\beta = (k_B T)^{-1}$, $f(\mathbf{Q})$ is the magnetic form factor, and $\hat{Q}_\alpha$ is the α-direction cosine of $\mathbf{Q}$. The dynamic structure factor can be written as

$$S^{\alpha}(\mathbf{Q},\omega)=(g^2\mu^2)^{-1}\chi^{\alpha}(\mathbf{Q})F^{\alpha}(\mathbf{Q},\omega) \ , \tag{2}$$

where $\chi(\mathbf{Q})$ describes the static spin correlations and $F(\mathbf{Q},\omega)$ is the spectral weight function that describes the spin dynamics.

The functional forms of $\chi(\mathbf{Q})$ and $F(\mathbf{Q},\omega)$ are reasonably well understood for certain regions of Q and T. At low temperatures, the only type of spin fluctuations that occur are the transverse spin waves which have energies of $\hbar\omega_q$ with $\mathbf{Q}=\mathbf{G}\pm\mathbf{q}$, where $\mathbf{G}$ is a reciprocal-lattice vector. Here, $\chi(\mathbf{q})$ is proportional to $\langle S^z\rangle/\omega_q$ and $F(\mathbf{q},\omega)$ assumes the form of δ functions in $(\omega\pm\omega_q)$. With increasing temperature, the spin-wave energies renormalize downward in energy and begin to be damped out in time due to spin-wave—spin-wave interactions. $\chi(\mathbf{q})$ retains the same form while $F(\mathbf{q},\omega)$ is usually assumed to take the form of a double Lorentzian peaking at $\omega=\pm\omega_q$ and with a half-width Γ that describes the spin-wave lifetime. As the temperature approaches T_c, the interactions become increasingly important and the proper description of $F(\mathbf{q},\omega)$ is not known. Above T_c, the long-wavelength spin waves no longer exist; the spin fluctuations at small q are well described by diffusion theory and $F(\mathbf{q},\omega)$ becomes a single Lorentzian centered at $\omega=0$. In this $T>T_c$ region, several approximate forms have been suggested for $F(\mathbf{q},\omega)$ that are also applicable at large q. One of the more interesting of these was obtained recently by Lindgård[10,11] using a Green's-function approach to describe the spin motion combined with a mode-mode—coupling approximation for the damping. To lowest order, he obtains a two-pole solution which corresponds to a damped-harmonic-oscillator form:

$$F(\mathbf{q},\omega)=\frac{2}{\pi}\langle\omega_q^2\rangle\frac{\beta_q}{(\omega^2-\langle\omega_q^2\rangle)^2+4\beta_q^2\omega^2} \ . \tag{3}$$

Here, $\langle\omega_q^2\rangle$ is the second moment of the frequency distribution and β_q is the damping parameter related to the relaxation time of the random forces. The two poles of the Green's function occur at $\pm\alpha_q+i\beta_q$ with $\langle\omega_q^2\rangle=\alpha_q^2+\beta_q^2$. Equation (3) reduces to the correct limits at low and high temperatures and includes correlations via the damping so that it can be expected to have a wide range of applicability. At low temperatures, $\beta_q\rightarrow0$ and there are poles only at $\omega=\pm\omega_q$, where $\hbar\omega_q$ is the spin-wave energy. For $T>T_c$, the line shape at small q becomes approximately Lorentzian centered on $\omega=0$, while peaks appear at larger q with peak positions given by

$$\omega_{peak}^2=\langle\omega_q^2\rangle-2\beta_q^2 \ . \tag{4}$$

The damped-harmonic-oscillator function given in Eq. (3) has been successfully used by Lindgård[10,11] to describe the spin-fluctuation data of EuO and EuS for $T\geq T_c$. We also find this function useful in describing the present data.

III. EXPERIMENTAL RESULTS

The measurements were made at the HB-2 triple-axis spectrometer at the High Flux Isotope Reactor at the Oak Ridge National Laboratory. The constant-Q mode of operation was used with a fixed final energy of either 1 or

3.6 THz. The scattered beam was filtered to remove higher-order wavelengths either by polycrystalline beryllium at 1 THz or pyrolytic graphite at 3.6 THz. Both the monochromator and analyzer were pyrolytic graphite with mosaic spreads of about 25'. The 3.6-THz data were taken with horizontal collimation of 40' before and after the sample, while measurements were made with both 40'—sample—40' and 20'—sample—20' collimation at 1 THz.

The single-crystal sample of ^{160}Gd with a volume of approximately 3 cm^3 and a mosaic spread of about 25' was mounted on the spectrometer with a $\langle110\rangle$ crystal-axis vertical. Measurements were made out to the zone boundaries in the $\langle00l\rangle$ and $\langle h00\rangle$ directions. Sample temperatures were maintained by a Displex refrigerator and measured with a silicon-diode thermometer. Data were obtained at fixed temperatures of 9, 100, 200, 250, 273, 282, 287, 292, 297, and 320 K.

The contrasting behavior of the magnetic excitation spectra at small and large q is illustrated in Figs. 1 and 2. the small q [$\mathbf{Q}=(0,0,1.9)$, $\mathbf{q}=\mathbf{Q}-(0,0,2)$] behavior is shown in Fig. 1 for four temperatures near T_c. The 250-K spectrum shows the creation and annihilation spin-wave peaks and a clearly resolved elastic peak. The spectra at lower temperatures are similar to this except that the spin-wave peaks are separated more in energy and the elastic peak increases in intensity with decreasing temperature, becoming an order of magnitude more intense at the lowest temperature. This temperature-dependent elastic scattering is not understood but may arise from domain-wall scattering. In the data analysis it is simply fitted to a Gaussian form and excluded from all energy integrations. With increasing temperature the spin-wave peaks remain clearly resolved up to 287 K, while the lower-intensity elastic peak becomes unresolved. At 292 K ($T\simeq T_c$), the spin-wave peaks become unresolved and appear as a single peak centered at zero energy. Qualitatively, this is the expected behavior for long-wavelength spin waves for which the energies should follow the mac-
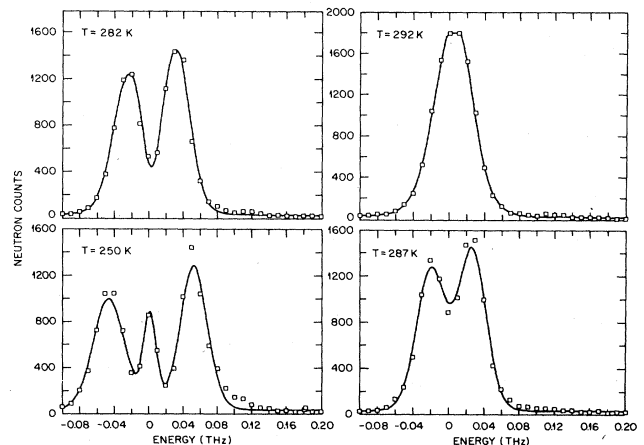

FIG. 1. Magnetic excitation spectrum of Gd for a few selected temperatures at small q [$\mathbf{Q}=(0,0,1.9)$]. The solid curves are least-squares-fitted to Eq. (5) with a damped-harmonic-oscillator spectral weight function.
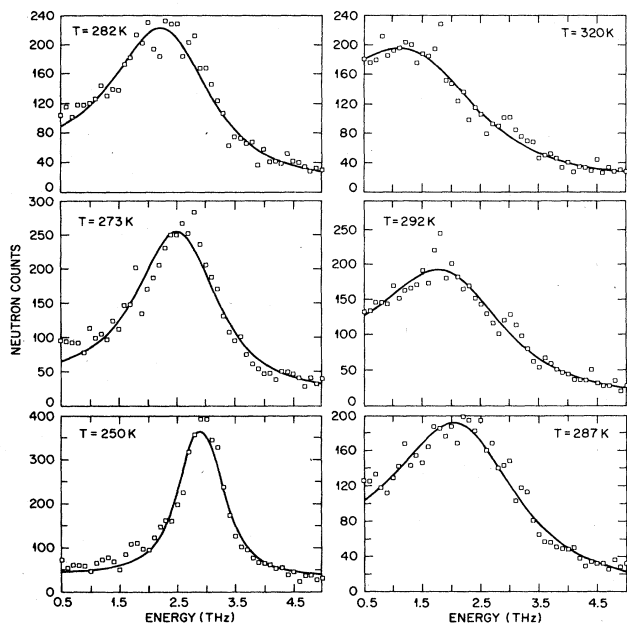
FIG. 2. Magnetic excitation spectrum of Gd for a few temperatures at large q [Q=(0,0,3.0)]. The solid curves were fitted in the same way as for Fig. 1.

roscopic magnetization and vanish at T_c.

The different behavior at large q is illustrated by Fig. 2, which shows excitation spectra at Q=(0,0,3.0) (q=1.0) for several temperatures near T_c. The 250-K spectrum shows a well-defined spin-wave peak of nearly Lorentzian shape at 2.9 Thz. The data at lower temperatures are similar, except that the spin-wave peaks occur at slightly higher energies and the background becomes an order of magnitude smaller at the lowest temperature. In contrast to the small-q data, for which line broadening was barely detectable, the line broadening here is appreciable and strongly temperature dependent. As the temperature is increased, the spin-wave peak decreases slowly in energy and becomes considerably broader and asymmetrical with extra intensity shifted into the low-energy region. A peak at finite energy remains even at 320 K (T/T_c = 1.09). However, it should be noted that the data shown in Figs. 1 and 2 are raw intensity data which include the background, the detailed balance factor, the instrumental resolution, etc. These may distort the intensity distribution so that a peak appears in $I(\mathbf{q},\omega)$ even in the absence of a peak in $F(\mathbf{q},\omega)$. The solid curves shown in these figures were least-squares-fitted to a constant background plus a Gaussian central peak (where required) plus a magnetic intensity given by

$$I(\mathbf{q},\omega) = I_0 \int_{\Delta\mathbf{q}} \int_{\Delta\omega} d(\Delta\mathbf{q}) d(\Delta\omega) R(\Delta\mathbf{q},\Delta\omega) \frac{k'}{k}$$

$$\times \omega(n_\omega + 1) F(\mathbf{q},\omega) g(E) . \qquad (5)$$

Here, I_0 is the amplitude of the intensity distribution and the double integral represents a convolution with the instrumental resolution $R(\Delta\mathbf{q},\Delta\omega)$. $g(E)$ is that fraction of

the total monitor count given by neutrons with the incident energy E. With an unfiltered beam incident on the monochromator, $g(E)$ is a significant correction, especially at low incident energies. It must be carefully determined for each monochromator from the integrated intensities of the higher-order-wavelength Bragg reflections from a well-characterized powder sample. For the present experimental arrangement, $g(E)$ was obtained from measurements on polycrystalline silicon and diamond. The data were fitted to Eq. (5) using both the damped-harmonic-oscillator and the double-Lorentzian forms for $F(\mathbf{q},\omega)$. Equally good fits were obtained when the damping was small, i.e., at low temperature or at small q. However, when the damping becomes large, especially as T approaches T_c, the damped-harmonic-oscillator form provides a significantly better fit, as is shown in Fig. 3. Here, the solid curve labeled DHO represents the damped-harmonic-oscillator fit and the dashed curve labeled DL is the double-Lorentzian fit. The corresponding X^2 values are 1.3 and 2.4. Clearly, the double-Lorentzian fit fails to reproduce the observed skewing of the spectrum that shifts extra intensity into the low-energy regions. As a result the fitted peak position shifts to lower energy than is actually observed. By contrast, the damped-harmonic-oscillator fit describes the data remarkably well. The solid curves shown in Figs. 1 and 2 also represent the damped-harmonic-oscillator fitting.

The data taken into the $\langle h00 \rangle$ direction present certain difficulties. The acoustic and optic spin-wave branches are observed separately only at small q. Further out in the zone, peaks from both branches appear in a constant-q scan and as the temperature increases the peaks merge and become unresolved. This behavior is illustrated by Fig. 4, which shows spectra taken at Q=(0.3,0,3) for a few selected temperatures. At 9 K the acoustic and optic spin-wave peaks appear at about 2.8 and 4.7 THz, respectively. These broaden and merge together at elevated temperatures, so that fits to the data do not give sensible results above about 250 K. Because of this problem the
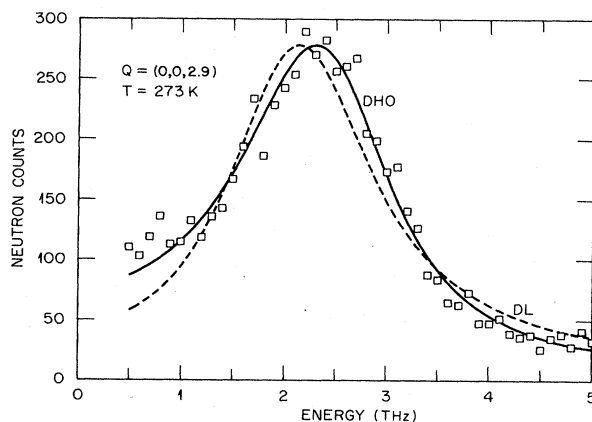

FIG. 3. Comparison of the damped-harmonic-oscillator (solid line) and double-Lorentzian (dashed line) fitting to the Gd data at large q and high T. The X^2 values are 1.3 and 2.4, respectively.
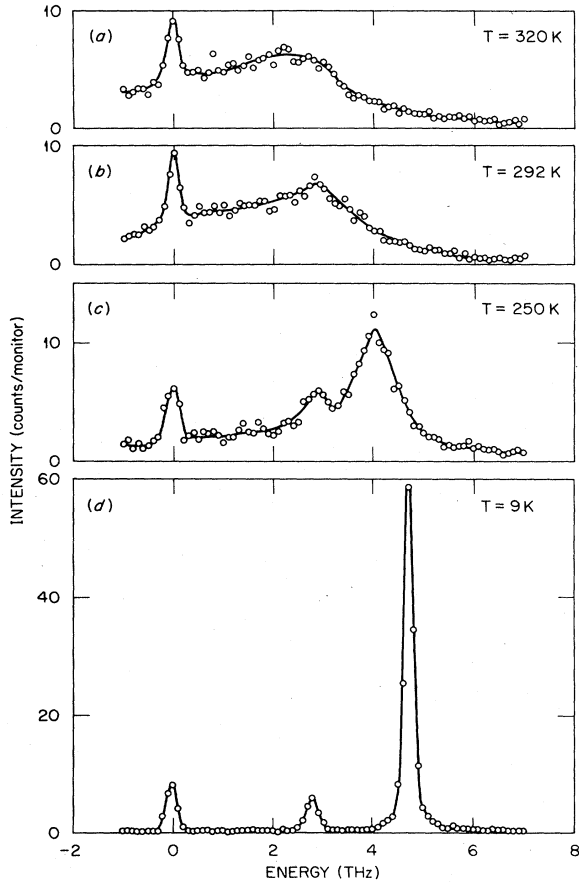
FIG. 4. Temperature dependence of the magnetic excitation spectrum of Gd in the $\langle h00 \rangle$ direction at $\mathbf{Q}=(0.3,0,3)$. The peaks near 2.7 and 4.8 THz at 9 K correspond to the acoustic and optic spin-wave branches.

FIG. 5. Temperature dependence of the parameters β_q and ω_q at small q [$\mathbf{Q}=(0,0,1.85)$] and large q [$\mathbf{Q}=(0,0,2.9)$].

$\langle h00 \rangle$ data have not been analyzed. However, these data show behavior similar to that observed at large q in the $\langle 00l \rangle$ direction. At elevated temperatures, there is pronounced peak broadening, skewing of the intensity distribution toward low energies, and the persistence of a peak at finite energy above T_c at 320 K.

The $\langle 00l \rangle$ data for the entire q and T regions of measurement were fitted with the damped-oscillator spectral weight function and the fitted parameters are given in Tables I—III. Here we take $\omega_q = (\langle \omega_q^2 \rangle)^{1/2}$.

The temperature dependences of the parameters ω_q and β_q are shown in Fig. 5, which again reveals the contrasting behavior of the small-q and large-q excitation spectra. The small-q behavior is shown in Fig. 5(a) for $\mathbf{Q}=(0,0,1.85)$. Here, ω_q decreases rapidly with increasing temperature, while β_q remains very small and temperature independent almost to T_c, where it increases rapidly. At large q [Fig. 5(b)], ω_q decreases more slowly and β_q increases more rapidly with increasing temperature.

The q dependences of ω_q and β_q are shown in Fig. 6 for a few selected temperatures. At the lower temperatures, β_q is small at all q and ω_q then corresponds to the spin-wave frequency. However, for $T \geq 250$ K, β_q becomes an appreciable fraction of ω_q over a large part of the zone.
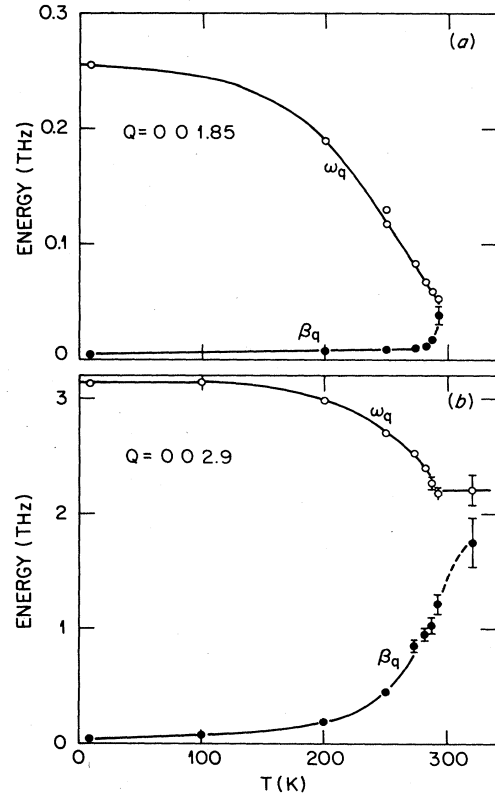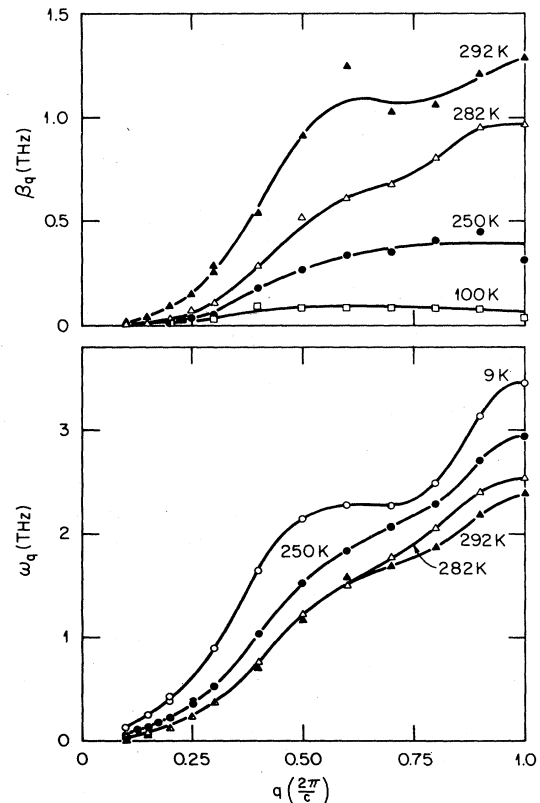

FIG. 6. q dependence of the parameters β_q and ω_q at a few selected temperatures.

TABLE I. Magnetic parameters for Gd [$E' = 3.6$ THz, 40'—sample—40', $Q = (0,0,2 + q)$, $C = 50.8$ counts b^{-1}].

T (K)	q $(2\pi/c)$	I_0 (THz^{-1})	ω_q (THz)	β_q (THz)	T (K)	q $(2\pi/c)$	I_0 (THz^{-1})	ω_q (THz)	β_q (THz)
9	0.2	163	0.38	0.07		0.6	13.8	1.63	0.51
	0.3	51.5	0.89	0.03		0.7	11.6	1.85	0.52
	0.4	30.9	1.64	0.08		0.8	9.8	2.11	0.59
	0.5	23.3	2.14	0.03		0.9	9.4	2.53	0.85
	0.6	19.0	2.28	0.02		1.0	7.6	2.68	0.75
	0.7	17.1	2.27	0.01	282	0.3	42.2	0.37	0.11
	0.8	15.5	2.49	0.06		0.4	23.9	0.76	0.29
	0.9	12.3	3.13	0.04		0.5	17.6	1.22	0.52
	1.0	7.9	3.45	0.01		0.6	13.8	1.51	0.61
100	0.2	101	0.37	0.02		0.7	11.7	1.77	0.68
	0.3	36.3	0.87	0.03		0.8	10.3	2.05	0.81
	0.4	21.7	1.56	0.09		0.9	9.3	2.40	0.95
	0.5	18.1	2.10	0.08		1.0	8.2	2.53	0.97
	0.6	15.1	2.28	0.08	287	0.3	63.9	0.37	0.20
	0.7	13.3	2.35	0.09		0.4	24.9	0.70	0.34
	0.8	10.4	2.53	0.08		0.5	17.7	1.16	0.62
	0.9	8.7	3.15	0.08		0.6	13.7	1.46	0.68
	1.0	7.0	3.40	0.04		0.7	11.9	1.70	0.77
200	0.2	65.5	0.30	0.01		0.8	10.4	1.96	0.90
	0.3	31.0	0.72	0.07		0.9	9.0	2.27	1.03
	0.4	16.6	1.33	0.16		1.0	8.4	2.56	1.24
	0.5	14.6	1.89	0.25	292	0.3	45.1	0.34	0.29
	0.6	11.8	2.15	0.26		0.4	26.2	0.70	0.54
	0.7	9.9	2.30	0.24		0.5	19.2	1.17	0.91
	0.8	8.4	2.54	0.30		0.6	15.5	1.58	1.24
	0.9	5.6	3.00	0.19		0.7	12.2	1.68	1.03
	1.0	3.9	3.22	0.09		0.8	10.7	1.87	1.06
250	0.3	42.1	0.52	0.06		0.9	9.3	2.18	1.21
	0.4	21.4	1.03	0.18		1.0	8.3	2.39	1.29
	0.5	16.4	1.52	0.27					
	0.6	14.2	1.83	0.34	320	0.3	36.6	0.39	0.64
	0.7	12.1	2.07	0.36		0.4	23.9	0.99	1.56
	0.8	10.0	2.29	0.41		0.5	17.5	1.19	1.34
	0.9	8.1	2.71	0.45		0.6	14.7	1.56	1.61
	1.0	5.9	2.93	0.32		0.7	11.2	1.54	1.16
273	0.3	44.7	0.42	0.09		0.8	11.0	2.06	1.78
	0.4	23.0	0.84	0.23		0.9	9.5	2.21	1.75
	0.5	17.5	1.31	0.42		1.0	7.6	2.17	1.54

Under these conditions, ω_q is no longer the peak position, which is given by Eq. (4) as $\omega_{\text{peak}} = (\langle \omega_q^2 \rangle - 2\beta_q^2)^{1/2}$. The spin-wave frequency then corresponds to ω_{peak} rather than ω_q. Thus, the ω_q-versus-q data shown in the lower part of Fig. 6 do not represent the spin-wave dispersion relations of Gd at elevated temperatures. The actual dispersion relations appear in Fig. 7, which shows the q dependence of ω_{peak} for a few representative temperatures. At 292 K, peaks appear at finite frequencies only for $q \geq 0.7(2\pi/c)$; the dashed line here represents the collapse of the spectral distribution into a single peak at zero frequency for the smaller q values.

In the long-wavelength limit, the spin-wave energy can be expanded in even powers of q, i.e.,

$$\hbar\omega_{\text{peak}} = A + Dq^2 + \cdots , \tag{6}$$

where A is an energy gap due to anisotropy and D is the spin-wave-stiffness constant. For Gd, this relation is valid for $T \leq 250$ K, as shown in Fig. 8 where the solid lines are fitted to Eq. (6) with the parameters given in the inset. At temperatures higher than 250 K, the spin-wave interactions become increasingly important and the q dependence becomes more nearly $q^{5/2}$. At T_c, $\omega_{\text{peak}} = 0$ at small q, but both ω_q and β_q follow a $q^{5/2}$ dependence, in agreement with dynamic scaling predictions.

TABLE II. Magnetic parameters for Gd [$E'=1$ THz, 40'—sample—40', $Q=(0,0,2-q)$, $C=1.8$ counts b^{-1}].

T (K)	q $(2\pi/c)$	I_0 (THz^{-1})	ω_q (THz)	β_q (THz)
9	0.10	18.0	0.126	0.006
	0.15	6.8	0.255	0.004
	0.20	5.1	0.424	0.005
200	0.10	7.2	0.111	0.007
	0.15	4.2	0.189	0.007
	0.20	2.3	0.331	0.013
	0.25	2.0	0.517	0.031
250	0.10	7.5	0.058	0.003
	0.15	5.5	0.130	0.008
	0.20	2.3	0.221	0.015
	0.25	2.6	0.376	0.041

TABLE III. Magnetic parameters for Gd. [$E'=1$ THz, 20'—sample—20', $Q=(0,0,2-q)$, $C=1.0$ counts b^{-1}].

| T (K)	q $(2\pi/c)$	I_0 (THz^{-1})	ω_q (THz)	β_q (THz)
250	0.10	4.8	0.53	0.004
	0.15	2.9	0.117	0.008
	0.20	2.0	0.212	0.015
	0.25	1.5	0.353	0.040
273	0.10	5.0	0.039	0.004
	0.15	2.6	0.083	0.010
	0.20	1.8	0.156	0.018
	0.25	1.3	0.272	0.042
282	0.10	5.2	0.032	0.006
	0.15	2.6	0.067	0.011
	0.20	1.5	0.129	0.026
	0.25	1.2	0.245	0.071
287	0.10	4.8	0.027	0.005
	0.15	2.7	0.059	0.017
	0.20	1.6	0.119	0.037
	0.25	1.1	0.223	0.081
	0.30	0.8	0.36	0.15
	0.35	0.5	0.52	0.19
292	0.10	4.5	0.023	0.017
	0.15	2.6	0.053	0.038
	0.20	1.6	0.126	0.092
	0.25	1.1	0.224	0.15
	0.30	0.9	0.37	0.26
	0.35	0.8	0.57	0.43
297	0.10	3.7	0.026	0.05
	0.15	2.6	0.076	0.17
	0.20	1.4	0.21	0.43
	0.25	1.2	0.52	1.1
	0.30	1.5	0.85	1.5
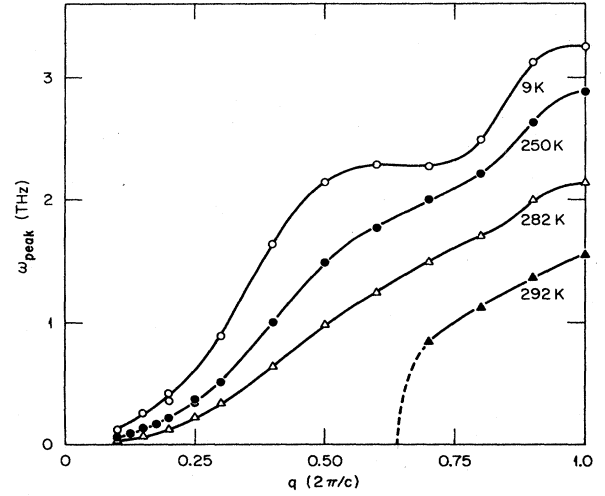
FIG. 7. q dependence of the spin-wave frequency [$\omega_{peak}=(\langle\omega_q^2\rangle-2\beta_q^2)^{1/2}$] at a few fixed temperatures. The dashed line at 292 K represents a collapse of ω_{peak} to zero below $q=0.7(2\pi/c)$.

As the temperature goes above T_c the spin motion becomes diffusive and the spectral weight function at small q becomes a Lorentzian centered at zero frequency, i.e.,

$$F(\mathbf{q},\omega)=\frac{1}{\pi}\frac{\Gamma_q}{\omega^2+\Gamma_q^2} ,\qquad(7)$$

where Γ_q is the inverse relaxation time. In this regime, the damped-harmonic-oscillator function of Eq. (3) assumes approximately this form with $\Gamma_q=\langle\omega_q^2\rangle/2\beta_q$. This approximation was tested by fitting the small-q data

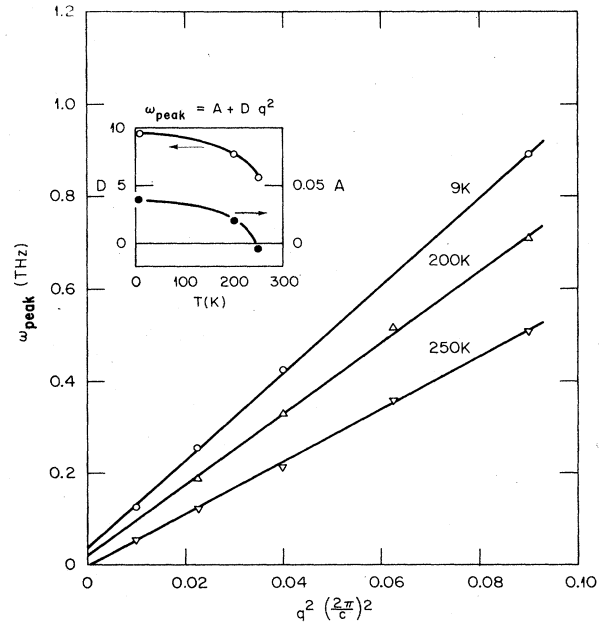FIG. 8. Small-q behavior of ω_{peak} for $T\leq250$ K. The inset shows the temperature dependence of the parameters obtained by fitting to $\omega_{peak}=A+Dq^2$.
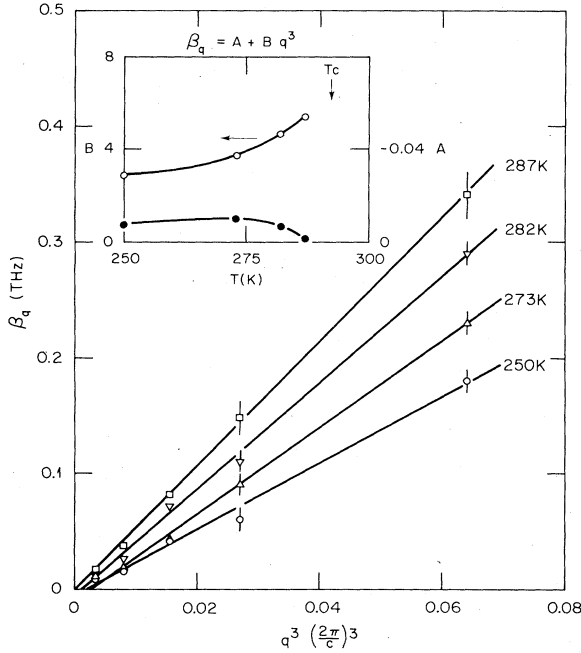
FIG. 9. Small-q behavior of β_q at elevated temperatures. The inset shows the temperature dependence of the parameters obtained by fitting to $\beta_q = A + Bq^3$.

at 297 and 320 K using both spectral weight functions. The Γ_q values agreed within 10% for all of the observed q values at 297 K and to $q = 0.5(2\pi/c)$ for the 320-K data. The parameter of Tables I and III can therefore be used to obtain the Lorentzian widths of the spectral distribution above T_c. Even though Γ_q exhibits a $q^{5/2}$ dependence at T_c, the q dependence becomes more pronounced above T_c, where it is best described by $\Gamma_q = Aq^2 + Bq^4$. This is qualitatively in accord with the approximation[18]

$$\hbar\Gamma_q = \Lambda q^2 r_1^2(\kappa_1^2 + q^2) , \qquad (8)$$

where $r_1^2\kappa_1^2 = (T - T_c)/T$ and $r_1^2 = \frac{1}{3}(S+1)D\beta$. It is known that this temperature dependence is much too strong as $T \rightarrow T_c$, but the results at 320 K are consistent with Eq. (8) with $\Lambda = 4.3$ THz$-(2\pi/c)^{-2}$.

The small-q dependence of the damping parameter is shown in Fig. 9, where the solid lines are fitted to $\beta_q = A + Bq^3$ with the parameters shown in the inset. Over this temperature range, $B(T) = 1.55 T^{*-0.32}$, where $T^* = (T_c - T)/T_c$.

IV. CALIBRATION OF THE DATA

The data were placed on an absolute basis by use of an internal calibration based on the integrated spin-wave intensities at 9 and 100 K. The integrated cross section for spin-wave creation is given by[18]

$$\left[\frac{d\sigma}{d\Omega}\right]_{\text{sw}} = \left[\frac{e^2\gamma}{mc^2}\right] f^2(\mathbf{Q})(n_q+1)(1+\hat{Q}_z^2)\frac{1}{2}S , \qquad (9)$$

where n_q is defined by $[\exp(\hbar\omega_q\beta) - 1]^{-1}$. The calibration constant C is obtained by comparing this with the fitted expression for $I(\mathbf{q},\omega)$ given in Eq. (5). C is defined by

$$C\left[\frac{d\sigma}{d\Omega}\right]_{\text{sw}} = \int_0^\infty d\omega \frac{I(\mathbf{q},\omega)}{g(E)} , \qquad (10)$$

where the integral is taken from 0 to ∞ because only spin-wave creation is included in $(d\sigma/d\Omega)_{\text{sw}}$. Equation (10) combined with Eq. (5) is readily integrable because both $F(\mathbf{q},\omega)$ and $R(\Delta q, \Delta\omega)$ are normalized functions and $F(\mathbf{q},\omega)$ is finite only for $\omega = \pm\omega_q$ at these low temperatures. We obtain

$$\int_0^\infty d\omega \frac{I(\mathbf{q},\omega)}{g(E)} = \frac{1}{2}I_0\omega_q(n_q + 1) . \qquad (11)$$

To evaluate Eq. (9) we need only the magnitude and orientation of the spin and the magnetic form factor. Magnetization data[19] for Gd yield a saturation moment of $7.55\mu_B$/atom, i.e., $0.55\mu_B$ larger than the $7\mu_B$ expected from the half-filled $4f$ shell. However, form-factor measurements[20] show that the moment density can be logically separated into diffuse and localized components which are identified as the conduction-electron and $4f$-electron contributions, respectively. The data are consistent with a localized moment of $7\mu_B$/atom. The relative magnetizations at 9 and 100 K then correspond to ordered spin magnitudes of 3.5 and 3.2, respectively. The temperature dependence of the moment orientation has been determined from Bragg scattering measurements.[21,22] Between T_c and the spontaneous-spin-reorientation temperature, $T_R = 235$ K, the moment is parallel to the c axis. Below T_R the moment direction moves away from the c axis and lies on the surface of a cone with semiapex angle ψ. At $T = 9$, 100, and 200 K, $\psi = 40°$, 59°, and 71°, respectively. [For spin waves propagating along $\langle 00l \rangle$, $(1 + \hat{Q}_z^2) = 1 + \cos^2\psi$.] The calibration constants obtained using these results and the form-factor data of Moon et al.[20] are included in Tables I and II. Low-temperature data were not taken for the experimental conditions of Table III; these data were calibrated by intercomparison of overlapping data at $T = 250$ K. The average calibration constants obtained for the data of Tables I, II, and III are 50.8, 1.8, and 1.0 counts monitor^{-1} b^{-1}, respectively.

V. MAGNETIC SUSCEPTIBILITY

At elevated temperatures, the cross section given by Eq. (1) can be integrated over energy directly by using the approximation $\hbar\omega\beta(n_\omega + 1) = 1$. Even though this is true only for small $\hbar\omega\beta$, it remains a reasonable approximation for the integration because $F(\mathbf{q},\omega)$ is symmetric in ω, so that the intensity lost on the energy-gain side is recovered on the energy-loss side. One obtains, for the integrated cross section,

$$\frac{d\sigma}{d\Omega} = \left[\frac{e^2\gamma}{mc^2}\right] f^2(\mathbf{Q})\frac{k_BT}{g^2\mu^2}\sum_\alpha (1 - \hat{Q}_\alpha^2)\chi^\alpha(\mathbf{q}) . \qquad (12)$$

With the same approximation, the energy integration of Eq. (5) yields

$$\int_{-\infty}^{\infty} d\omega \frac{I(\mathbf{q},\omega)}{g(E)} = \frac{I_0}{\hbar\beta} \ . \tag{13}$$

For $T < T_c$, $\mathcal{X}^{\alpha}(\mathbf{q})$ is defined relative to the direction of the ordered moment, which is taken as the z axis. Assuming that the transverse fluctuations are equal in this uniaxial system, the α sum becomes

$$(1+\hat{Q}_z^2)\mathcal{X}^t(\mathbf{q})+(1-Q_z^2)\mathcal{X}^l(\mathbf{q}) \ ,$$

where the superscripts refer to the transverse and longitudinal susceptibilities. At low temperatures, the longitudinal susceptibility is negligible and, for $T \geq T_R = 235$ K, the moment is parallel to the c axis and $\mathcal{X}^l(q)$ is not observed for Q along $\langle 00l \rangle$. We therefore use $(1+\hat{Q}_z^2)\mathcal{X}^t(\mathbf{q})$ at all $T < T_c$. The susceptibility can then be expressed in terms of the fitted parameters by

$$\frac{k_B T}{g^2\mu^2}\mathcal{X}^t(\mathbf{q}) = \frac{I_0}{C\hbar\beta(e^2\gamma/mc^2)f^2(\mathbf{Q})(1+\hat{Q}_z^2)} \ . \tag{14}$$

In molecular-field theory, the transverse susceptibility below T_c is given by[18]

$$\frac{k_B T}{g^2\mu^2}\mathcal{X}^t(\mathbf{q}) = \frac{\langle S^z \rangle}{\hbar\beta\omega_q} \ , \tag{15}$$

where ω_q is the spin-wave energy. A comparison between the observed and calculated inverse susceptibilities is shown in Fig. 10. Here, the data points are calculated from Eq. (14) and the solid lines correspond to Eq. (15) with $\langle S^z \rangle$ taken from the magnetization data. Fortuitously, a single line represents both temperatures in both Figs. 10(a) and 10(b). The agreement at 9 and 100 K is to

be expected since the calibration was obtained using spin-wave theory, which yields the same result as Eq. (15). At 200 K the data lie slightly above the calculated line, but the agreement is such as to provide confidence in the calibration procedure. At 250 K, agreement is not obtained and we assume that Eq. (15) no longer applies. Since spin-wave theory indicates that $\hbar\omega_q = Dq^2$ at small q, Fig. 10 can be considered as an inverse-susceptibility—versus—q^2 plot. The 250-K data would then correspond to a Lorentzian shape for $\mathcal{X}(q)$ with a finite-inverse-range parameter. In molecular-field theory, the susceptibility at $T > T_c$ can be written in a Lorentzian form,[18]

$$\frac{k_B T}{g^2\mu^2}\mathcal{X}^t(\mathbf{q}) = \frac{R}{\kappa_1^2+q^2} \ , \tag{16}$$

where $R = S/D\beta$ and $\kappa_1^2 = 3RT^*/S(S+1)$ with $T^* = (T-T_c)/T$. The inverse-range parameter κ_1 then approaches zero with a $T^{*1/2}$ dependence and remains zero below T_c. The behavior of the 250-K data shown in Fig. 10 indicates that this divergence of the correlation length does not occur in Gd. Instead, κ_1 remains finite below T_c. This same result was obtained by Child[23] using the quasielastic scattering method. The observed susceptibilities at elevated temperatures were fitted to Eq. (16) in the small-q region and the fitted parameters are given in Table IV. For $T > T_c$, we use Eq. (14) with the c axis defined as the z direction; $\mathcal{X}^t(\mathbf{q})$ then corresponds to the correlation of spin components perpendicular to the c axis. If we assume the low-temperature values of $D = (9.5$ THz$)(2\pi/c)^{-2}$ and $S = \frac{7}{2}$, then the calculated susceptibility parameters are $R = 0.0077\,T(2\pi/c)^2$ and $\kappa_1 = 0.038(T-T_c)^{1/2}$. The observed and calculated κ_1 parameters are in good agreement for $T > T_c$, but the observed R parameters are approximately a factor of 2 too small at all T except for $T = 320$ K. This discrepancy is not understood.

VI. SPIN WAVES ABOVE T_c?

We now address the question that actually provided the motivation for this study: do propagating spin-wave modes persist above T_c for Gd? We recognize that this question is not easily answered. Inherent to the neutron technique is the problem of instrumental resolution, which dictates some assumption for the scattering law in order to extract the parameters that describe the spin fluctuations. In the case of Gd, we find that a damped-
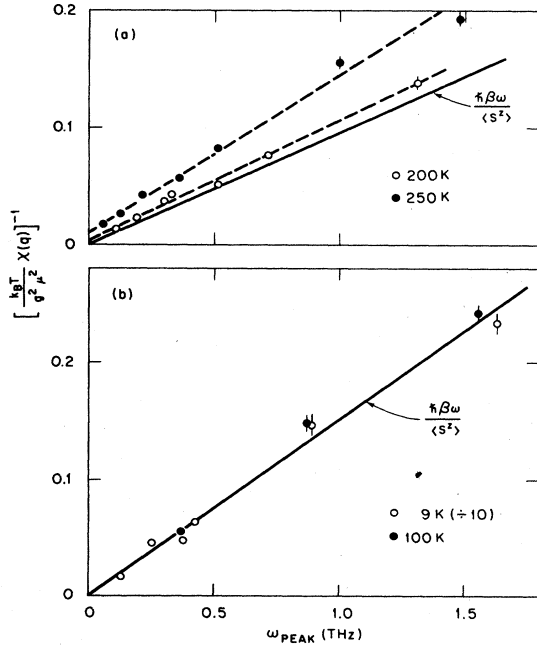

FIG. 10. Comparison of the observed transverse susceptibility (data points) with that calculated from molecular-field theory (solid lines). The dashed lines in (a) serve only as a guide to the eye; however, they correspond to Lorentzian $\mathcal{X}(q)$'s with finite-inverse-range parameters.

TABLE IV. Magnetic susceptibility parameters of Gd. $[(k_B T/g^2\mu^2)\mathcal{X}(q)=R/(\kappa_1^2+q^2).]$

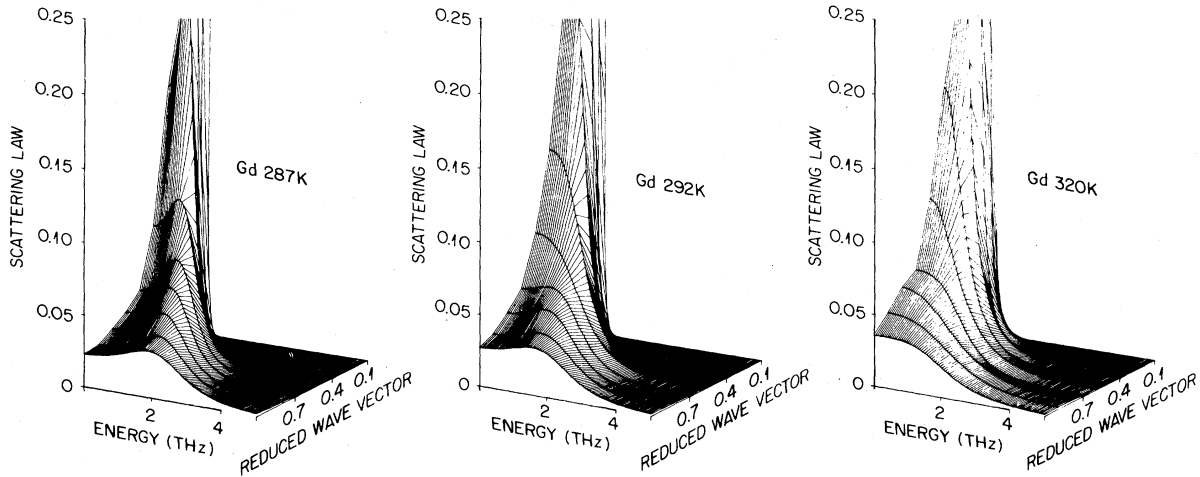| T (K)	R $(2\pi/c)^2$	κ_1 $(2\pi/c)$
250	1.24	0.10
273	1.09	0.08
282	1.06	0.08
287	1.02	0.07
292	1.01	0.07
297	1.14	0.10
320	1.75	0.18

FIG. 11. Three-dimensional projections of the scattering law for Gd along $\langle 00l \rangle$ at three temperatures near T_c. The vertical scale is in absolute units as given by Eq. (17).

harmonic-oscillator type of scattering law describes the data remarkably well over a large range of q and T, and have parametrized the data accordingly. In order to decide between diffusive or propagating spin-wave behavior, it is desirable to examine $F(\mathbf{q},\omega)$ rather than the observed $I(\mathbf{q},\omega)$ which contains other distorting features. We have therefore calculated $F(\mathbf{q},\omega)$ from the fitted parameters and present the scattering law at three temperatures near T_c in Fig. 11. The plots are in absolute units of $b\,\mathrm{THz}^{-2}$ and represent the expression

$$\frac{I_0 F(\mathbf{q},\omega)}{2Cf^2(\mathbf{Q})} = \left[\frac{e^2\gamma}{mc^2}\right]^2 \frac{k_B T}{g^2\mu^2}\chi(\mathbf{q})F(\mathbf{q},\omega)\hbar\beta . \tag{17}$$

Actually, the scattering-law behavior shown here is only slightly different from the $I(\mathbf{q},\omega)$ behavior described earlier and shown in Figs. 1 and 2. At 287 K there are spin-wave peaks at finite energies at all q. At 292 K $(\sim T_c)$ the spectrum below $q=0.7(2\pi/c)$ peaks at $\omega=0$; peaks at finite ω occur only at the larger q values. Finally, at 320 K there are no peaks at finite ω for any q, although the zone-boundary spectrum is distinctly non-Lorentzian. We conclude that there are no spin waves propagating along $\langle 00l \rangle$ at 320 K $(T/T_c = 1.09)$.

The same conclusion can be drawn from the fitted parameters if Eq. (4) is taken as the criterion for propagating spin-wave behavior. According to Eq. (4) peaks appear in the spectrum at finite energies only for $\omega_q > \sqrt{2}\beta_q$. Figure 12 shows the ratio of β_q/ω_q versus q for the same three temperatures near T_c. The horizontal line across the figure at $\omega_q = \sqrt{2}\beta_q$ represents the boundary between propagating spin waves (below) and diffusive, or at least nonpropagating, behavior (above). All of the 287-K data lie in the spin-wave region, while all of the 320-K data lie above the boundary and peak at zero frequency. The 292-K data lie close to the boundary over most of the zone and dip into the spin-wave region only for $q \geq 0.7$ $(2\pi/c)$.

VII. DISCUSSION

We have measured the magnetic excitation spectra of Gd over the entire Brillouin zone in the $\langle h\,00 \rangle$ and $\langle 00l \rangle$ directions in the temperature range from 9 to 320 K. Over this entire region of q and T, the $\langle 00l \rangle$ data are well described by the damped-harmonic-oscillator form of the spectral weight function. This is not a surprising result because this function reduces to the correct limits at both low and high temperature and was expected to have a wide range of applicability. It is a very convenient function for data analysis and allows the reliable parametrization of a large body of data with parameters corresponding to an intensity I_0, a damping term β_q, and the second moment of the frequency distribution $\langle \omega_q^2 \rangle$. The spin-
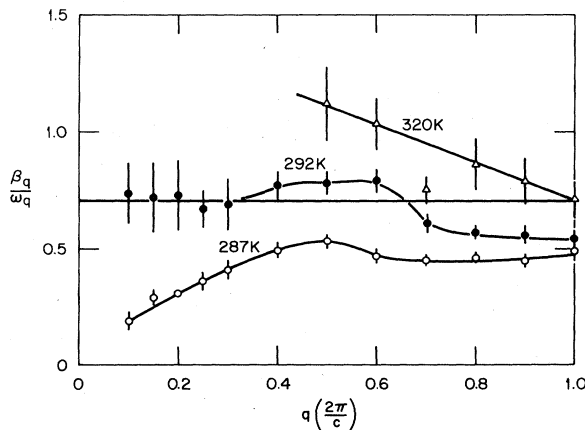

FIG. 12. q dependence of the ratio β_q/ω_q for three temperatures near T_c. The horizontal line is the boundary between peaks at finite frequency $(\beta_q/\omega_q < \sqrt{2}/2)$ and a single peak at zero frequency $(\beta_q/\omega_q \geq \sqrt{2}/2)$.

wave frequency is given by $(\langle\omega_q^2\rangle-2\beta_q^2)^{1/2}$. We observe spin-wave peaks at finite frequency over the entire zone at 287 K ($\sim 0.98 T_c$), but only for $q\geq 0.7(2\pi/c)$ at 292 K ($\sim T_c$). There are no spin-wave peaks at any q at 320 K ($\sim 1.09 T_c$).

This last observation is perhaps surprising since spin-wave peaks apparently occur at $T=2T_c$ for the similar Heisenberg systems EuO and EuS. However, the existence of spin waves above T_c depends on the energetics of the spin system relative to the thermal fluctuations provided by $k_B T_c$. If the characteristic energy of the spin system is taken as the zone-boundary spin-wave energy, then for both EuO and EuS that energy is nearly the same as $k_B T_c$, while for Gd in the $\langle 00l\rangle$ direction it is only about $0.6 k_B T_c$. This difference probably accounts for the presence of spin waves above T_c for EuO and EuS and their absence in Gd along $\langle 00l\rangle$. If this is the case, then spin waves above T_c should also occur in Gd in the $\langle h00\rangle$ and $\langle hh0\rangle$ directions where the zone-boundary spin-wave energy is equal to $k_B T_c$. This persistence of $\langle h00\rangle$ spin waves can actually be seen in Fig. 4, which clearly shows a peak at finite energy at $T=320$ K. Additional measurements along these directions with higher spin-wave energies will be made in the near future.

The data were internally calibrated using the integrated intensities of the low-temperature spin waves. This allows the determination of the q-dependent magnetic susceptibilities in absolute units by energy integration of the spectral distributions. The observed magnetic susceptibilities agree reasonably well with molecular-field theory for $T\leq 200$ K and for $T>T_c$. However, disagreement is found in the region from 250 to 292 K where a small but finite inverse range parameter is observed.

ACKNOWLEDGMENTS

*Present address: Department of Physics, Keio University, Yokohama 233, Japan.

[1]For a brief survey, see T. Moriya, J. Magn. Magn. Mater. 31-34, 10 (1983).

[2]Y. J. Uemura, G. Shirane, O. Steinsvoll, and J. Wicksted, Phys. Rev. Lett. 51, 2322 (1983).

[3]G. Shirane, O. Steinsvoll, Y. J. Uemura, and J. Wicksted, J. Appl. Phys. 55, 1887 (1984).

[4]J. W. Lynn, Phys. Rev. Lett. 52, 775 (1984).

[5]H. A. Mook and J. W. Lynn, J. Appl. Phys. 57, 3006 (1985).

[6]M. Blume and J. Hubbard, Phys. Rev. B 1, 3815 (1970).

[7]J. Hubbard, J. Phys. C 4, 53 (1971).

[8]S. W. Lovesey and R. A. Meserve, J. Phys. C 6, 79 (1973).

[9]A. P. Young and B. S. Shastry, J. Phys. C 15, 4547 (1982).

[10]P. Lindgård, J. Appl. Phys. 53, 1861 (1982).

[11]P. Lindgård, Phys. Rev. B 27, 2980 (1983).

[12]T. Oguchi, K. Terakura, and N. Hamada, J. Phys. F 13, 145 (1983).

[13]H. A. Mook, Phys. Rev. Lett. 46, 508 (1981).

[14]H. G. Bohn, A. Kollmar, and W. Zinn, Phys. Rev. B 30, 6504 (1984).

[15]J. W. Cable, N. Wakabayashi, and R. M. Nicklow, J. Appl. Phys. 52, 2231 (1981).

[16]P. Lindgård, Phys. Rev. B 17, 2348 (1978).

[17]W.C. Koehler, H. R. Child, R. M. Nicklow, H. G. Smith, R. M. Moon, and J. W. Cable, Phys. Rev. Lett. 24, 16 (1970).

[18]W. Marshall and S. W. Lovesey, Theory of Thermal Neutron Scattering (Clarendon, Oxford, 1971).

[19]H. E. Nigh, S. Legvold, and F. H. Spedding, Phys. Rev. 132, 1092 (1963).

[20]R. M. Moon, W. C. Koehler, J. W. Cable, and H. R. Child, Phys. Rev. B 5, 997 (1972).

[21]J. W. Cable and E. O. Wollan, Phys. Rev. 165, 733 (1968).

[22]J. W. Cable and W. C. Koehler, J. Appl. Phys. 53, 1904 (1982).

[23]H. R. Child, Phys. Rev. B 18, 1247 (1978).